3. Dynamic Analysis of Q-Baller

The mechatronic design of Q-Baller has defined the system properties for us to establish its dynamic model. The modeling is based on the combined characteristics of both mechanical and electronic behaviors. Models in different forms will be established for different control purposes. The model of Q-Baller will go through zero-input stability and controllability analysis. The dynamic analysis of Q-baller will be crucial for the design and implement of suitable controller.

3.1. Coordinate System and Vector Definition

Q-Baller only contains 2 parts. However, the dynamics of Q-baller is not simple because of the 4 friction drive we used. The motion of the spherical wheel is separated from the robot body, indicating that different coordinate systems should be used for the analysis of motion.

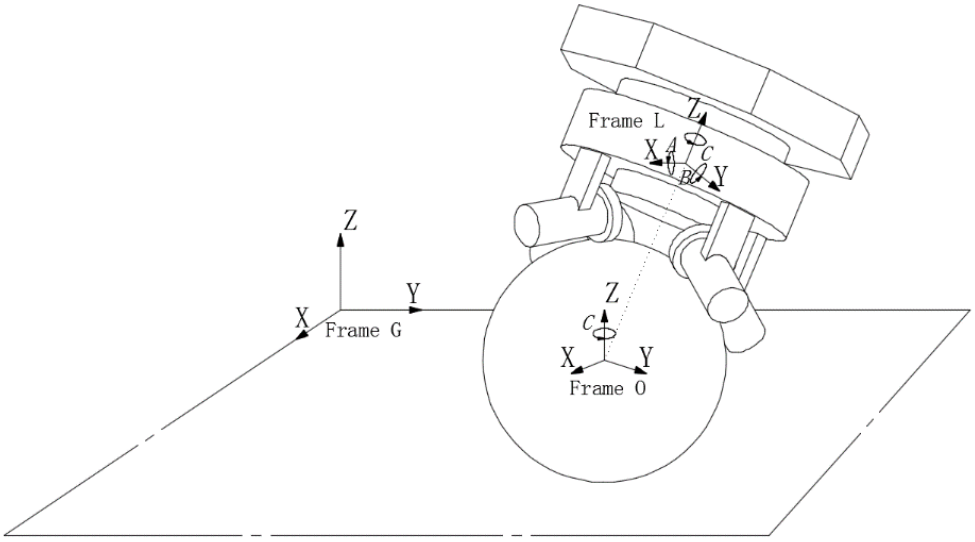

Figure 3.1. Different Coordinate Frames of the System

After careful selections, the Cartesian coordinate frames of the system used in the modeling process are depicted in Fig. 3.1., the 3 frequently used coordinate systems are shown below.

1). The Ground Frame (Frame G) will be set up by the time the robot starts running;
2). The origin of the Origin Frame (Frame O) is at the center of the ball and it takes form after the orientation conversion around the Z axis (Yawing) from Frame G;
3). The Local Frame (Frame L) takes form after the Pitching and Rolling of the coordinate system, its center is located at the center of the ball;

The origins of Frame O and Frame L are both located at the center of the ball, while in Fig.3.1 Frame L is moved away only for clearer presentation purpose.

The Q-baller system includes multiple geometric and input parameters which will be used during the modeling process. Fig. 3.2 describes the defined vectors in the system as shown below:

1). $\overrightarrow{\mathrm{V_M}}$ stands for the vector pointing from the origin of Frame L to the center of mass of the robot body:

$$\overrightarrow{V_M} = [H_X \quad H_Y \quad H_Z]^T$$

2). $\overrightarrow{V_R}$ and $\overrightarrow{V_w}$ points from the origin to the contact point of the ground and one of the friction Omni-Wheels respectively:

$$\overrightarrow{V_R} = [0 \quad 0 \quad -R]^T;\ \overrightarrow{V_w} = r * \begin{bmatrix} IB & IB & -IB & -IB \\ -IB & IB & IB & -IB \\ IC & IC & IC & IC \end{bmatrix}$$

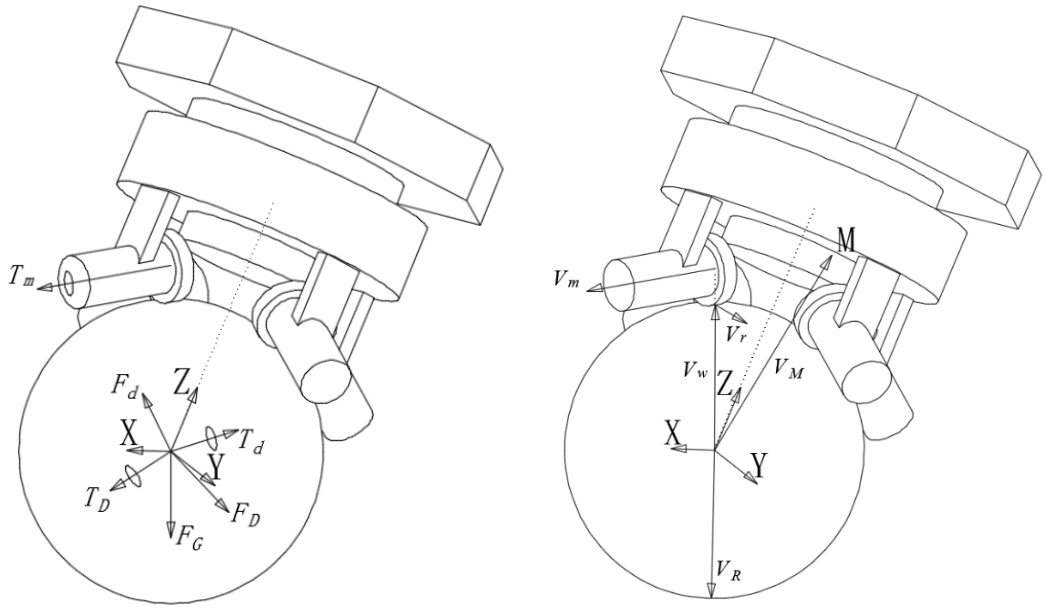

Figure 3.2. Force and Geometric Vectors of the System

3). $\overrightarrow{V_m}$ and $\overrightarrow{V_r}$ stands for the positive direction of the rotary velocity and the positive translational velocity direction at the contact point on the Omni-Wheel from one of the motors respectively:

$$\overrightarrow{V_m} = \begin{bmatrix} IX & -IX & -IX & IX \\ -IY & -IY & IY & IY \\ -IZ & IZ & -IZ & IZ \end{bmatrix};\ \overrightarrow{V_r} = \begin{bmatrix} IA & IA & -IA & -IA \\ IA & -IA & -IA & IA \\ 0 & 0 & 0 & 0 \end{bmatrix}$$

4). $\overrightarrow{T_m}$ is the actuating torque effect on the robot body from one of the motors:

$$\overrightarrow{T_m} = \begin{bmatrix} IX & -IX & -IX & IX \\ -IY & -IY & IY & IY \\ -IZ & IZ & -IZ & IZ \end{bmatrix}$$

5). $\overrightarrow{F_G}$ is the gravity force of the Ball-Bot's body (*origins from the Center of Mass of the body*):

$$\overrightarrow{F_G} = [0 \quad 0 \quad -g * M]^T$$

6). $\overrightarrow{T_d}, \overrightarrow{F_d}, \overrightarrow{T_D}, \overrightarrow{F_D}$ are the 4 exterior perturbation inputs (forces and torques) acting on the body and the ball (which are under Frame G) which will be used as process noises during simulation:

$$\overrightarrow{T_d} = \begin{bmatrix} T_{dx} \\ T_{dy} \\ T_{dz} \end{bmatrix};\ \overrightarrow{F_d} = \begin{bmatrix} F_{dx} \\ F_{dy} \\ F_{dz} \end{bmatrix};\ \overrightarrow{T_D} = \begin{bmatrix} T_{Dx} \\ T_{Dy} \\ T_{Dz} \end{bmatrix};\ \overrightarrow{F_D} = \begin{bmatrix} F_{Dx} \\ F_{Dy} \\ F_{Dz} \end{bmatrix}$$

Here R is the radius of the ball and r is the radius of the ball, which are scalar values; M is the mass of the robot body; IX, IY, IZ, IA, IB and IC are intermediate geometric numbers.

Note that $\overrightarrow{V_w}, \overrightarrow{V_m}, \overrightarrow{V_r}$ and $\overrightarrow{T_m}$ are sets of 3×4 matrixes because there are 4 motors in total, and direction vectors are unit vectors.

3.2. Dynamic Modeling

The Q-Baller motion is defined in the 3D space due to the coupling effect of different attitude states and the application purpose of the robot. For this reason, Q-Baller's dynamic system is modeled through Lagrangian Method. Since modeling is crucial for dynamic analysis and controller design, we established a flexible and detailed model by taking exclusive information from the system's mechatronic model into consideration.

To adopt a Lagrangian Method [3-1], we first choose the generalized coordinates according to the following assumptions:

1). the Ball-Bot will always be on the ground;
2). there is no slipping between any of the contact surfaces;
3). the body never loses contact with the ball;

The coordinate vectors chosen only include 5 states in total:

$$q = [A \quad B \quad C \quad X \quad Y]^T \tag{3.1}$$

As shown in (3.1), A, B, C are the Euler Angles describing the rotation of the robot body around axis X (Rolling), Y (Pitching), Z (Yawing) in Frame L, and X, Y are the accumulated distance of the Ball-Bot traveled along X and Y directions in Frame O which are derived from the rotation of the ball. Some of the terms are derived from the coordinate vectors. Here are the terms for the Lagrange Equations:

$$W_{B-L} = M_J[\dot{A} \quad \dot{B} \quad \dot{C}]^T \tag{3.2}$$

$$W_{b-O} = \left[-\frac{\dot{Y}}{R} \quad \frac{\dot{X}}{R} \quad 0\right]^T \tag{3.3}$$

$$V_G = C_O^G V_O = C_L^G * [\dot{X} \quad \dot{Y} \quad 0]^T \tag{3.4}$$

Here C_L^G is the coordinate conversion matrix from the local to Frame G. The other coordinate conversion matrixes are similar (For example: C_X^Y is the coordinate transformation matrix from X frame to Y frame.). M_J is the Jacobian Matrix transforming the Euler Angle rates to the angular velocity of the robot body. Some of these conversion matrixes are shown below in (3.5), (3.6) [3-2, 3-3]:

$$M_J = \begin{bmatrix} 1 & 0 & -sin(B) \\ 0 & cos(A) & sin(A)\,cos(B) \\ 0 & -sin(A) & cos(A)\,cos(B) \end{bmatrix} \tag{3.5}$$

$$C_L^G = \begin{bmatrix} cos(C) & -sin(C) & 0 \\ sin(C) & cos(C) & 0 \\ 0 & 0 & 1 \end{bmatrix} \begin{bmatrix} cos(B) & 0 & sin(B) \\ 0 & 1 & 0 \\ -sin(B) & 0 & cos(B) \end{bmatrix} \begin{bmatrix} 1 & 0 & 0 \\ 0 & cos(A) & -sin(A) \\ 0 & sin(A) & cos(A) \end{bmatrix} \tag{3.6}$$

According to the Lagrangian formulation, we have the following equations which govern the motion of the Ball-Bot's entire mechanical system [3-1, 3-3]:

$$T_L = \frac{1}{2} V_G^T (M + m) V_G \tag{3.7}$$

$$T_R = \frac{1}{2}(W_{B-L}^T J_B W_{B-L}) + \frac{1}{2}\left(W_{b-O}^T J_b W_{b-O}\right) \tag{3.8}$$

$$T_C = M\left(V_G^T C_L^G\right)(W_{B-L} \times V_M) \tag{3.9}$$

$$V = -F_G C_L^G V_M \tag{3.10}$$

$$L = T_L + T_R + T_C - V \tag{3.11}$$

$$Q_I = W_{b-O}^T C_L^O (T_W + C_G^L T_d) + W_{B-L}^T (-T_W + C_G^L T_D) + V_G^T (F_D + F_d) \quad (3.12)$$

$$Q_D = \frac{1}{2} V_G^T \left(C_L^G B_{BL} + B_{bL}\right) V_G + \frac{1}{2} (W_{B-L}^T B_{BR} W_{B-L}) + \frac{1}{2} \left(W_{b-O}^T B_{bR} W_{b-O}\right) \quad (3.13)$$

And finally the Lagrange Equation:

$$\frac{d}{dt}\left(\frac{\partial L}{\partial \dot{q}_i}\right) - \left(\frac{\partial L}{\partial q_i}\right) = \left(\frac{\partial (Q_I dt)}{\partial (dq_i)}\right) - \left(\frac{\partial Q_D}{\partial \dot{q}_i}\right) \quad (for \;\; i = 1,2 \ldots 5) \quad (3.14)$$

Here $T_L + T_R + T_C$ make up the kinematic energy of the whole system including translation, rotary movement plus the coupling effect since the rotary coordinate of the robot body does not origin from its center of mass; V accounts for the potential energy from the non-conservative forces – the gravity forces, for which the Zero-Potential-Level is set at the horizontal plane that goes through the center of the ball; Q_I stands for the virtual work caused by internal and exterior inputs; and Q_D is the energy dissipation term according to Rayleigh Dissipation Function caused by viscosity dampers in the system. (J and B terms are rotary inertias and viscosity dampers measured in the components' local frames.)

The following part is the modeling of the mechatronic system and the constraints to complete the modeling of the whole mechatronic system. According to the geometry of the robot system, the working torque T_W as the sum of the motor outputs acting on the ball:

$$T_W = -\frac{R}{r}\left[T_{m_{x+y+}} \quad T_{m_{x+y-}} \quad T_{m_{x-y-}} \quad T_{m_{x-y+}}\right]^T \quad (3.15)$$

The subscript of the motor's torque T_m indicates the direction the torque tends to make the whole robot move to in the Frame O. Each T_m is determined by the dynamics of the DC motor [3-4, 3-5]:

$$\frac{T_{s_0} U}{U_0} - T_m = J_w \dot{\omega} + b_w \omega + \frac{60 T_{s_0}}{2\pi n_{0_0}} \omega \quad (3.16)$$

Equation (3.16) has omitted the fast dynamics from the inductances in the motor, and it is simplified by the free spin velocity n_{0_0}, stalling torque T_{s_0} and nominal voltage U_0 according to the typical steady performance plot of DC motors.

According to the nonslip condition, the contact point velocity at the friction wheel and the ball should be identical. Thus, for each motor the velocity equation should be:

$$\omega_j = V_{r_j}^T ((C_O^L W_{b-O}) \times V_{W_j} - W_{B-L} \times V_{W_j})/r \quad (3.17)$$

Where V_{XX_j} is the jth column of the V_{XX} matrix, and $j = 1,2,3,4$. The equations couple the electronic systems of the motors with the mechanical system of the robot.

3.3. Standard Presentation of Dynamic System

Previous system modeling layout indicated that the modeling process can cater to the special need of analyzing system with modeling inaccuracy, since we have allowed deviation of the center of mass, asymmetric rotary inertia and other flexibilities. Due to the complexity of the system, the modeling process was realized through computer calculation tools. For the complete system, we can assume that the states and the inputs are those as shown below:

$$x = \left[A \quad B \quad C \quad X \quad Y \quad \dot{A} \quad \dot{B} \quad \dot{C} \quad \dot{X} \quad \dot{Y}\right]^T \quad (3.18)$$

$$u = [U_{x+y+} \quad U_{x+y-} \quad U_{x-y-} \quad U_{x-y+}]^T \quad (3.19)$$

$$v = [T_D^T \quad F_D^T \quad T_d^T \quad F_d^T]^T \quad (3.20)$$

And the standard ODE functions are:

$$\dot{x} = f(x, u, v) \tag{3.21}$$

$$y = g(x, u, w) \tag{3.22}$$

The ODE functions describes the system as a whole – all of the information (structure, size, driver, etc.) are included in the ODE function. The nonlinear system is highly coupled and can hardly be analyzed directly through the equations of motions. To solve this problem, State-Space Presentation is adopted through linearizing the system to the following format [3-6]:

$$\dot{X_{SS}} = A_{SS}X_{SS} + B_{SS}U_{SS} \tag{3.23}$$

$$Y_{SS} = C_{SS}X_{SS} + D_{SS}U_{SS} \tag{3.24}$$

The equation shown above does not include process and measurement noises. For a realistic model in practical condition, the State-Space equations are shown as below:

$$\dot{X_{SS}} = A_{SS}X_{SS} + B_{SS}U_{SS} + E_{SS}V_{SS} \tag{3.25}$$

$$Y_{SS} = C_{SS}X_{SS} + D_{SS}U_{SS} + F_{SS}W_{SS} \tag{3.26}$$

Where V_{SS} and W_{SS} are process noise and measurement noise, respectively.

In the State-Space Matrix, C_{SS} is determined through control objective. For example, the corresponding Y_{SS} in the controllers for position control and velocity control are shown below:

$$Y_{Position} = \begin{bmatrix} A & B & C & X & Y & \dot{A} & \dot{B} & \dot{C} & \dot{X} & \dot{Y} \end{bmatrix}^T$$

$$Y_{Velocity} = \begin{bmatrix} A & B & C & \dot{A} & \dot{B} & \dot{C} & \dot{X} & \dot{Y} \end{bmatrix}^T$$

3.4. Characteristic of the Standard Model

The modeling process introduced before allow generations of varies models for different experiment and simulation purpose. Therefore, a standard model is selected to represent the general characteristics of the Q-Baller. The Standard model has symmetric physical properties and most of its features are idealistic. The system parameters we selected for the standard model are shown below in Table 3.1., which are selected according to the 3D model designed in the CAD software.

Height of the Center of Mass (H)	0.107 m	Mass of the Ball (m)	1.5 kg
Rotary Inertia of Omni-Wheel (J_W)	$1.25*10^{-5}$ kg-m^2	Radius of the Ball (R)	0.1 m
Mass of the Body (M)	6.4 kg	Radius of the Omni-Wheels (r)	0.024m
Damper on Body during Translation (b_{BL})	0.008 N-s/m	Damper on Ball during Translation (b_{bL})	0.002 N-s/m
Rotary Inertia of Ball (J_b)	0.00975 kg-m^2	Rotary Damper on Ball (b_{bR})	0.01 N-s/rad
Rotary Inertia of Body on X axis (j_{XX})	0.1488 kg-m^2	Rotary Damper on Body on X axis (b_{XX})	0.02 N-s/rad
Rotary Inertia of Body on Y axis (j_{YY})	0.1512 kg-m^2	Rotary Damper on Body on Y axis (b_{YY})	0.02 N-s/rad
Rotary Inertia of Body on Z axis (j_{ZZ})	0.0746 kg-m^2	Rotary Damper on Body on Z axis (b_{ZZ})	0.01 N-s/rad
Standard Stalling Torque of Motor (T_{S0})	2.5 N-m	Standard No Load Speed of Motor (n_{00})	2000 r/min
Standard Voltage of Motor (U_0)	12V	Rotary Damper on Omni-Wheel (b_W)	0.005 N-s/rad

Table 3.1. Properties of the Standard Model

As the system has multiple equilibrium points and the states are highly coupled, single linearization will not be able to show the overall feature of the system. Through observation at several of its linearization points, it is easy to realize the high nonlinearity of the system due to the coupled states. For example, when linearized at an arbitrary point (not equilibrium):

$$x = [0.0873 \quad 0.0873 \quad 0 \quad 0 \quad 0 \quad 0 \quad 0 \quad 0 \quad 0 \quad 0]^T$$

$$u = [0 \quad 0 \quad 0 \quad 0]^T$$

The State-Space matrixes A_{SS} and B_{SS} reflect the mentioned features clearly, as can be recognized from the data presented below:

$$A_{SS} = \begin{bmatrix} 0 & 0 & 0 & 0 & 0 & 1 & 0 & 0 & 0 & 0 \\ 0 & 0 & 0 & 0 & 0 & 0 & 1 & 0 & 0 & 0 \\ 0 & 0 & 0 & 0 & 0 & 0 & 0 & 1 & 0 & 0 \\ 0 & 0 & 0 & 0 & 0 & 0 & 0 & 0 & 1 & 0 \\ 0 & 0 & 0 & 0 & 0 & 0 & 0 & 0 & 0 & 1 \\ 68.15 & -0.04 & 0 & 0 & 0 & -8.17 & 0.02 & 0.16 & -0.20 & -80.65 \\ -1.05 & 66.02 & 0 & 0 & 0 & 0.03 & -7.96 & 0.14 & 78.42 & 0.20 \\ 5.80 & 5.84 & 0 & 0 & 0 & -0.005 & -0.34 & -3.99 & 3.43 & -3.43 \\ 0.12 & -4.97 & 0 & 0 & 0 & -0.007 & 1.10 & 0.05 & -11.02 & -0.03 \\ 5.12 & -0.08 & 0 & 0 & 0 & -1.12 & 0.003 & 0.05 & -0.03 & -11.18 \end{bmatrix}$$

$$B_{SS} = \begin{bmatrix} 0 & 0 & 0 & 0 & 0 & 8.76 & -8.58 & -6.45 & 1.25 & 1.26 \\ 0 & 0 & 0 & 0 & 0 & -8.83 & -10.10 & 4.83 & 1.37 & -1.26 \\ 0 & 0 & 0 & 0 & 0 & -10.38 & 10.17 & -4.85 & -1.38 & -1.39 \\ 0 & 0 & 0 & 0 & 0 & 10.44 & 8.50 & 6.47 & -1.23 & 1.39 \end{bmatrix}^T$$

However, at the point where all of the states are zero, the State-Space matrixes A_{SS} and B_{SS} has shown weak coupling effect and nonlinearity, which are shown below:

$$A_{SS} = \begin{bmatrix} 0 & 0 & 0 & 0 & 0 & 1 & 0 & 0 & 0 & 0 \\ 0 & 0 & 0 & 0 & 0 & 0 & 1 & 0 & 0 & 0 \\ 0 & 0 & 0 & 0 & 0 & 0 & 0 & 1 & 0 & 0 \\ 0 & 0 & 0 & 0 & 0 & 0 & 0 & 0 & 1 & 0 \\ 0 & 0 & 0 & 0 & 0 & 0 & 0 & 0 & 0 & 1 \\ 69.27 & 0 & 0 & 0 & 0 & -8.23 & 0 & 0 & 0 & -81.08 \\ 0 & 67.60 & 0 & 0 & 0 & 0 & -8.04 & 0 & 79.12 & 0 \\ 0 & 0 & 0 & 0 & 0 & 0 & 0 & -3.98 & 0 & 0 \\ 0 & -5.17 & 0 & 0 & 0 & 0 & 1.11 & 0 & -11.12 & 0 \\ 5.30 & 0 & 0 & 0 & 0 & -1.13 & 0 & 0 & 0 & -11.27 \end{bmatrix}$$

$$B_{SS} = \begin{bmatrix} 0 & 0 & 0 & 0 & 0 & 9.68 & -9.44 & -5.68 & 1.32 & 1.34 \\ 0 & 0 & 0 & 0 & 0 & -9.68 & -9.44 & 5.68 & 1.32 & -1.34 \\ 0 & 0 & 0 & 0 & 0 & -9.68 & 9.44 & -5.68 & -1.32 & -1.34 \\ 0 & 0 & 0 & 0 & 0 & 9.68 & 9.44 & 5.68 & -1.32 & 1.34 \end{bmatrix}^T$$

This result indicates that the motion of Q-Baller can be handled more easily when it is close to the point where all states are zero – the Zero Point. Linear Controller will have better performance when closed to the Zero Point, while it may lose robustness when the states are away from the Zero Point.

3.5. Controllability and Observability

The controllability and observability analysis [3-6] are useful to test if the model, or in other words, the design satisfies the control prerequisites.

The controllability of Q-Baller may vary according to different states. From direct observation we can easily realize that if the robot's Pitch and Roll exceed certain extend, the friction drives will not be able to recover the system to stabilization. Therefore, we presume that the system will be controlled closed to the Zero Point.

According to the Controllability Theory, the rank of the controllability matrix of the Q-Baller is presented below:

$$rank(Q_c) = rank([B \quad AB \quad A^2B \quad \cdots \quad A^{n-1}B]) = 10 \tag{3.27}$$

Here, $n = 10$, and the result yielded from (3.27) is also 10. Therefore:

$$rank(Q_c) - n = 0 \tag{3.28}$$

This indicates that the system is fully controllable, leading to the acknowledged feasibility of the design model.

The observability of the model is judged from a more practical way, which is related to the system's actual setup: The electronic system of Q-Baller will support at least a Gyroscopic Sensor and an Accelerometer, which will detect $Y_{Sensor} = [A \quad B \quad C \quad \dot{A} \quad \dot{B} \quad \dot{C} \quad \ddot{X} \quad \ddot{Y}]^T$. And then we can achieve the $Y_{Position}$ through numerical integration. Simply from this view point we can draw the conclusion that the system is fully observable.

However, the sensor feedbacks may not be ideally reliable. For example, the state $X, Y, \dot{X}$ and $\dot{Y}$ achieve through Accelerometer may not be fully reliable due to the calculation error during integration and the signal noise. In a more realistic way, the actual observability of the system is more related to the reliability of the feedback.

3.6. Conclusion

Chapter 3 has introduced the dynamic modeling of the mechatronic system of Q-Baller. The modeling is thorough including almost all features (Motors, Friction Drives, Viscosities etc.) of Q-Baller. The final model is highly complex and nonlinear, which requires us to get familiar with it through experimenting rather than only looking at the governing equations.

The system shows low nonlinearity when the states are all zero, and therefore we named it as the Zero Point which will be used in our further studies. Some simple analysis about the controllability and observability of the system are performed. The final results proved that the system is fully controllable around the Zero Point. The modeling process has paved the road for the controller study, which will be discussed in the next chapter.

Reference:

[3-1]. Donald T. Greenwood: *Principle of Dynamics (2nd Edition),* ISBN-13: 978-0137099818, Pearson Education (1987)

[3-2]. Phil Kim, *Rigid Body Dynamics for Beginners: Euler angles & Quaternions*, ISBN-13: 978-1493598205, CreateSpace Independent Publishing Platform (2013)

[3-3]. G. V. Raffo, M. G. Ortega, and F. R. Rubio: *An Integral Predictive/nonlinear H ∞ Control Structure for a Quadrotor Helicopter*, Automatica, vol. 46, no. 1, pp. 29 – 39 (2010)

[3-4]. Abdulrahman A. A. Emhemed , Rosbi Bin Mamat: *Modelling and Simulation for Industrial DC Motor Using Intelligent Control*, Procedia Engineering Volume 41, 2012, Pages 420-425, International Symposium on Robotics and Intelligent Sensors 2012 (IRIS 2012)

[3-5]. Yongxing Hao, Manxiang Miao, Xiaoyan Luo: *Electric Drive Control (Chinese Edition),* ISBN-13: 978-560958620, Huazhong University of Science and Technology Press (2009)

[3-6]. Katsuhiko Ogata: *Modern Control Engineering (5th Edition)*, ISBN-13: 978-0136156734, Pearson Education (2009)